This article has been accepted for inclusion in a future issue of this journal. Content is final as presented, with the exception of pagination.

High-Performance Atomic-Layer-Deposited Indium Oxide 3-D Transistors and Integrated Circuits for Monolithic 3-D Integration

Mengwei Si, Zehao Lin, Zhizhong Chen, and Peide D. Ye, *Fellow, IEEE*

***Abstract*—In this work, we report the experimental demonstration of In_2O_3 3-D transistors coated on fin structures and integrated circuits by a back-end-of-line (BEOL) compatible atomic layer deposition (ALD) process. High-performance planar back-gate In_2O_3 transistors with high mobility of 113 $cm^2/V \cdot s$ and high maximum drain current (I_D) of 2.5 mA/μm are achieved by channel thickness engineering and postdeposition annealing. The high-performance ALD In_2O_3-based zero-V_{GS}-load inverter is demonstrated with a maximum voltage gain of 38 V/V and a minimum supply voltage (V_{DD}) down to 0.5 V. Top-gate indium oxide (In_2O_3) transistors by low-temperature ALD of both gate insulator and channel semiconductor are also demonstrated with I_D of 570 μA/μm and low subthreshold slope (SS) down to 84.6 mV/decade. ALD In_2O_3 3-D Fin transistors with the top-gate structure are then demonstrated, benefiting from the conformal deposition capability of ALD. These results suggest that ALD oxide semiconductors and devices have unique advantages and are promising toward BEOL-compatible monolithic 3-D integration for 3-D integrated circuits.**

***Index Terms*—3-D structure, atomic layer deposition (ALD), back-end-of-line (BEOL) compatible, indium oxide, oxide semiconductor, thin-film transistor.**

I. Introduction

OXIDE semiconductors are the leading semiconducting channel materials for flat-panel display applications [1], [2]. Recently, indium oxide (In_2O_3) or doped-In_2O_3, such as (indium gallium zinc oxide, IGZO), are being investigated as promising channel materials for back-end-of-line (BEOL) compatible transistors for monolithic 3-D integration [3], by both sputtering [4]–[13] and atomic layer deposition (ALD) [14]–[18], due to their high mobility, wide bandgap, low variability, and high stability. ALD-based oxide semiconductors [19]–[23] are of special interest due to the atomically smooth surface, ultrathin thickness, and the capability of conformal deposition on 3-D structures. Recently, high-performance back-gate ALD In_2O_3 transistors have been demonstrated with a high drain current over 2 mA/μm in both depletion-mode (D-mode) and enhancement-mode (E-mode) operations [15], [16]. The devices have ultrascaled channel thickness (T_{ch}) down to 0.7 nm, channel length down (L_{ch}) to 40 nm, low thermal budget below 400 °C, and stability in the H_2 environment, which are highly compatible with the BEOL process. Meanwhile, for many practical applications, a top-gate device structure is required for integrated circuits and other applications. However, how to form high-quality gate dielectric on top of ALD In_2O_3 and how to realize high-performance top-gate ALD In_2O_3 transistors remain unclear.

In this work, the performance of back-gate ALD In_2O_3 transistors is further enhanced by T_{ch} engineering and postdeposition annealing. An optimized T_{ch} is determined to be 2.2–2.5 nm, achieving record high mobility of 113 $cm^2/V \cdot s$ and record-high maximum drain current of 2.5 mA/μm at L_{ch} of 40 nm and $V_{DS} = 0.7$ V. The high-performance back-gate ALD In_2O_3 transistors-based zero-V_{GS}-load inverter is demonstrated with a maximum voltage gain of 38 V/V and a minimum supply voltage (V_{DD}) down to 0.5 V. Top-gate In_2O_3 transistors are also demonstrated by low-temperature ALD of both gate insulator and channel semiconductor. High-performance top-gate In_2O_3 transistors are realized with a maximum drain current (I_D) of 570 μA/μm and a low subthreshold slope (SS) down to 84.6 mV/decade. It is found that the deposition of hafnium oxide (HfO_2) as gate insulator at low temperature and postdeposition annealing in O_2 at low temperature are critical to annihilate defects that are generated during the formation of top dielectrics and top-gate electrodes. ALD In_2O_3 3-D Fin transistors with top-gate structures coated on SiO_2 fin structures are also demonstrated for the first time, taking advantage of conformal deposition of ALD on 3-D structures.

Manuscript received July 20, 2021; revised August 12, 2021; accepted August 15, 2021. This work was supported in part by the Semiconductor Research Corporation (SRC) through the nanoelectronic COmputing REsearch (nCORE) Innovative Materials and Processes for Accelerated Compute Technologies (IMPACT) Center and in part by the SRC/Defense Advanced Research Projects Agency (DARPA) Joint University Microelectronics Program (JUMP) Applications and Systems Driven Center for Energy-Efficient Integrated NanoTechnologies (ASCENT) Center. The review of this article was arranged by Editor S. Yu. *(Corresponding author: Peide D. Ye.)*

Mengwei Si was with the School of Electrical and Computer Engineering, Purdue University, West Lafayette, IN 47907 USA, and also with the Birck Nanotechnology Center, Purdue University, West Lafayette, IN 47907 USA. He is now with the Department of Electronic Engineering, Shanghai Jiao Tong University, Shanghai 200240, China.

Zehao Lin, Zhizhong Chen, and Peide D. Ye are with the School of Electrical and Computer Engineering, Purdue University, West Lafayette, IN 47907 USA, and also with the Birck Nanotechnology Center, Purdue University, West Lafayette, IN 47907 USA (e-mail: yep@purdue.edu).

Color versions of one or more figures in this article are available at https://doi.org/10.1109/TED.2021.3106282.

Digital Object Identifier 10.1109/TED.2021.3106282

0018-9383 © 2021 IEEE. Personal use is permitted, but republication/redistribution requires IEEE permission.
See https://www.ieee.org/publications/rights/index.html for more information.

Authorized licensed use limited to: Purdue University. Downloaded on September 08,2021 at 16:24:56 UTC from IEEE Xplore. Restrictions apply.

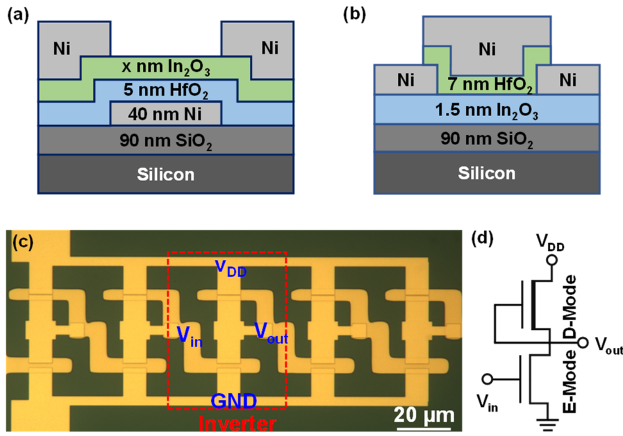

Fig. 1. Schematic of a planar In_2O_3 transistor with (a) back-gate and (b) top-gate structures. (c) Photograph image of an In_2O_3 zero-V_{GS}-load inverter in a five-stage ring oscillator. (d) Circuit diagram of a zero-V_{GS}-load inverter.

II. Experiments

Fig. 1 presents the schematic of planar (a) back-gate and (b) top-gate In_2O_3 transistors. The back-gate device structure is similar to previously reported in [15] and [16], which is used for circuit demonstration. The gate-stack consists of 40-nm Ni as gate metal, 5-nm HfO_2 as gate dielectric, 0.5–3.5-nm In_2O_3 as semiconducting channels, and 80-nm Ni as source/drain electrodes. The device fabrication process is similar to [15] and [16]. The fabricated devices were annealed in O_2, N_2, or forming gas (FG, 96% N_2/4% H_2) for 30 s at different temperatures from 250 °C to 350 °C according to the optimized annealing conditions achieved in [15]. Fig. 1(c) shows the photograph of a fabricated In_2O_3 zero-V_{GS}-load inverter in a five-stage ring oscillator. The circuit diagram of the In_2O_3 zero-V_{GS}-load inverter is shown in Fig. 1(d). D-mode and E-mode transistors could be achieved by threshold voltage (V_T) engineering, such as plasma treatment described in [17]. The E-mode device has a channel length (L_{ch}) of 2 μm, while L_{ch} of D-mode devices (L_D) varies from 0.1 to 0.3 μm to engineer the load resistance.

The gate-stack of planar top-gate In_2O_3 transistors, as shown in Fig. 1(b), includes 40-nm Ni as gate metal, 7-nm HfO_2 as gate dielectric, 1.5-nm In_2O_3 as the semiconducting channel, and 40-nm Ni as source/drain electrodes. The device fabrication starts with a standard cleaning of 90-nm SiO_2/p+ Si substrates. The 1.5-nm-thick In_2O_3 films were then deposited by ALD at 225 °C, using $(CH_3)_3In$ (TMIn) and H_2O as In and O precursors. Channel isolation was done by wet etching use concentrated HCl. The 40-nm Ni was then deposited by e-beam evaporation as S/D contacts. Then, HfO_2 was deposited by ALD at various temperatures of 120 °C/150 °C/200 °C, using $[(CH_3)_2N]_4Hf$ (TDMAHf) and H_2O as Hf and O precursors. The impact of ALD deposition temperature is discussed in great detail in the following section. The fabricated devices were annealed by rapid thermal annealing (RTA) in O_2 at different temperatures. 3-D Fin transistors with top-gate structures were fabricated on a SiO_2/Si substrate with SiO_2 fin structures. The top-gate dielectric of

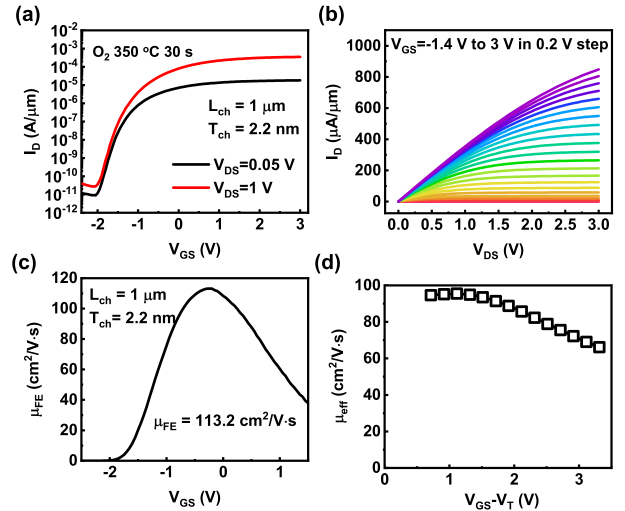

Fig. 2. (a) I_D–V_{GS} and (b) I_D–V_{DS} characteristics of a planar back-gate In_2O_3 transistor with L_{ch} of 1 μm and T_{ch} of 2.2 nm with O_2 annealing at 350 °C for 30 s. (c) μ_{FE} versus V_{GS} extracted from the maximum g_m at V_{DS} of 0.05 V from the transfer curve. (d) μ_{eff} versus V_{GS} extracted from the g_d from the output curve.

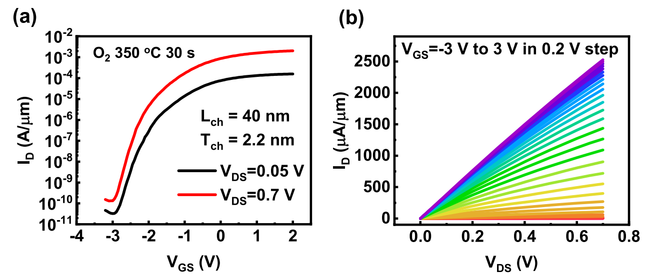

Fig. 3. (a) I_D–V_{GS} and (b) I_D–V_{DS} characteristics of a planar back-gate In_2O_3 transistor with L_{ch} of 40 nm and T_{ch} of 2.2 nm with O_2 annealing at 350 °C.

7-nm HfO_2 was formed by low-temperature ALD at 120 °C, which is critical to form top-gate devices.

III. Results and Discussion

Fig. 2(a) shows the I_D–V_{GS} characteristics of a planar In_2O_3 transistor with L_{ch} of 1 μm and T_{ch} of 2.2 nm with O_2 annealing at 350 °C for 30 s. Fig. 2(b) shows the corresponding I_D–V_{DS} characteristics of the same device, exhibiting high maximum I_D of 850 μA/μm even with L_{ch} of 1 μm and well-behaved drain current saturation at high V_{DS}. Such high I_D is the result of high field-effect mobility (μ_{FE}) of 113 cm^2/V·s, as shown in Fig. 2(c), extracted from the maximum transconductance (g_m) at V_{DS} of 0.05 V. Effective mobility (μ_{eff}) versus V_{GS} extracted from drain conductance (g_d) are presented in Fig. 2(d), which is consistent with μ_{FE}. Fig. 3(a) and (b) presents the I_D–V_{GS} and I_D–V_{DS} characteristics of an In_2O_3 transistor with L_{ch} of 40 nm and T_{ch} of 2.2 nm, exhibiting a high maximum I_D of 2.5 mA/μm under V_{DS} = 0.7 V and $V_{GS} - V_T$ = 4 V with optimized T_{ch} and annealing conditions. Further dielectric scaling is needed to realize $V_{GS} - V_T$ approaching V_{DS}.

The mobility of In_2O_3 in this work is significantly improved compared to other ALD-based oxide

Authorized licensed use limited to: Purdue University. Downloaded on September 08,2021 at 16:24:56 UTC from IEEE Xplore. Restrictions apply.

This article has been accepted for inclusion in a future issue of this journal. Content is final as presented, with the exception of pagination.

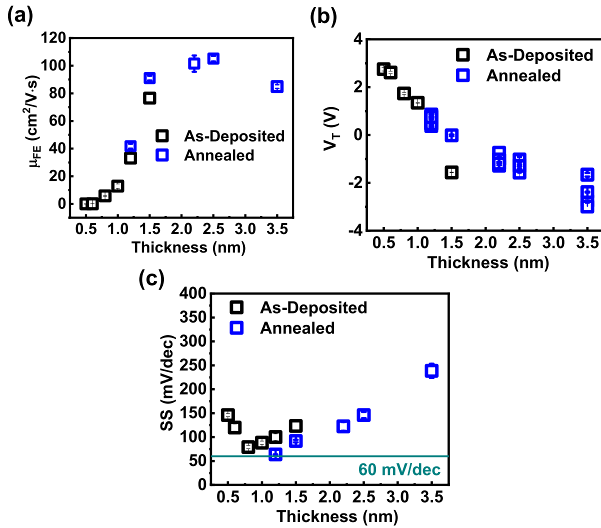

Fig. 4. (a) μ_{FE}, (b) V_T, and (c) SS versus T_{ch} extracted from as-deposited devices and devices with optimized annealing conditions.

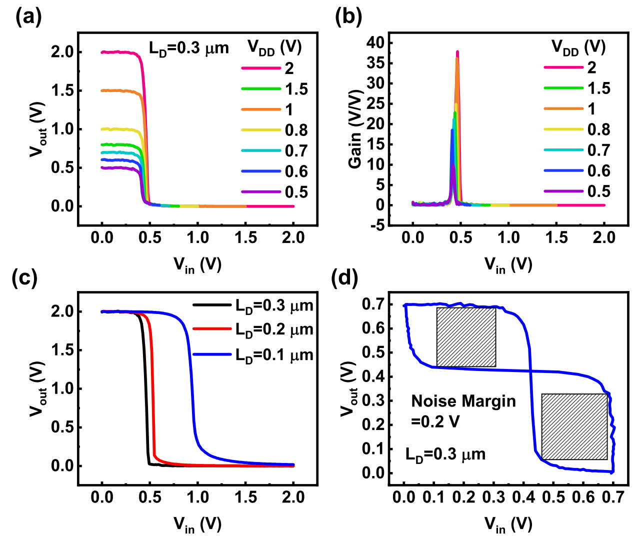

Fig. 5. (a) V_{out} versus V_{in} and (b) voltage gain of an In_2O_3 zero-V_{GS}-load inverter with L_D of 0.3 μm at different V_{DD}'s. (c) V_{out} versus V_{in} of In_2O_3 zero-V_{GS}-load inverters with different L_D's at V_{DD} of 2 V. (d) NM of the In_2O_3 zero-V_{GS}-load inverter as in (a) at V_{DD} of 0.7 V.

semiconductors [19]–[23]. Such high mobility is achieved by T_{ch} engineering and postdeposition annealing, as shown in Fig. 4(a). Average μ_{FE} > 100 $cm^2/V\cdot s$ is achieved with T_{ch} of 2.2–2.5 nm at optimized annealing conditions. μ_{FE} decreases rapidly with T_{ch} below 1 nm, most likely due to the enhanced surface scattering and quantum confinement effect on the band structure [14]. μ_{FE} decreases at T_{ch} above 3 nm due to the higher carrier concentration and weaker gate electrostatic control, as also shown in V_T versus T_{ch} in Fig. 4(b). Postdeposition annealing for the reduction of oxygen vacancies in as-deposited films is needed to tune V_T of devices with T_{ch} above 2 nm to obtain a sufficiently high on/off ratio. V_T of devices with certain T_{ch} can be controlled by annealing conditions, as shown in Fig. 4(b). Fig. 4(c) shows T_{ch}-dependent SS extracted from as-deposited devices and devices with optimized annealing conditions, exhibiting SS close to the thermal limit of 60 mV/decade at room temperature at T_{ch} $\sim$ 1 nm. The thickness-dependent SS indicates that the interface trap density D_{it} in the subthreshold region may be related to T_{ch}. However, the atomic configuration at the oxide/semiconductor interface does not have a T_{ch} dependence. Thus, the defect energy levels should not change with respect to the vacuum level. Therefore, the only possible reason is that the band structure of In_2O_3 is changing with T_{ch} (such as T_{ch}-dependent conduction band minimum, E_C) so that the Fermi level (E_F) alignment at the subthreshold region is changing. This result is consistent with previous theoretical analysis and density function theory (DFT) simulations [14].

Fig. 5(a) presents V_{out} versus V_{in} curve of an In_2O_3 zero-V_{GS}-load inverter with L_D of 0.3 μm at different V_{DD}'s from 2 down to 0.5 V, showing well-behaved voltage transfer characteristics. The voltage gains are given in Fig. 5(b), achieving a maximum voltage gain of 38 V/V at V_{DD} of 2 V. The midpoint voltage of the In_2O_3 zero-V_{GS}-load inverter can be engineered by tuning the load resistance and varying the channel length of the D-mode transistor, as illustrated in Fig. 5(c), providing the essential approach for V_{DD} and midpoint voltage

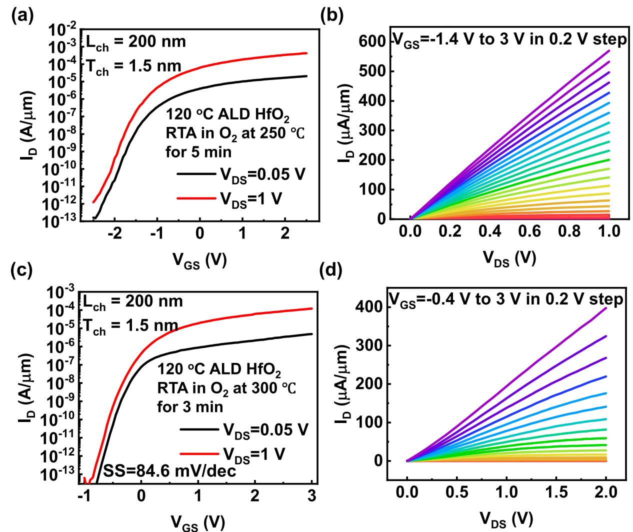

Fig. 6. (a) I_D–V_{GS} and (b) I_D–V_{DS} characteristics of a top-gate In_2O_3 transistor with L_{ch} of 200 nm, T_{ch} of 1.5 nm, 7-nm HfO_2 by ALD at 120 °C, and with RTA in O_2 at 250 °C for 5 min. (c) I_D–V_{GS} and (d) I_D–V_{DS} characteristics of a top-gate In_2O_3 transistor with L_{ch} of 200 nm, T_{ch} of 1.5 nm, 7-nm HfO_2 by ALD at 120 °C, and with RTA in O_2 at 300 °C for 3 min.

engineering accordingly. Therefore, a sufficiently large noise margin (NM) can be achieved at a low V_{DD} of 0.7 V, as shown in Fig. 5(d).

Fig. 6(a) and (b) shows the I_D–V_{GS} and I_D–V_{DS} characteristics of a top-gate In_2O_3 transistor with L_{ch} of 200 nm and T_{ch} of 1.5 nm. The HfO_2 gate dielectric in this device was deposited at 120 °C, and the device was annealed by RTA in O_2 at 250 °C for 5 min. The device exhibits well-behaved switching on and off characteristics, with a maximum I_D of 570 μA/μm. Fig. 6(c) and (d) shows the I_D–V_{GS} and I_D–V_{DS} characteristics of a top-gate In_2O_3 transistor with L_{ch} of 200 nm, T_{ch} of 1.5 nm, and with HfO_2 gate dielectric deposited at 120 °C and annealed by RTA in O_2 at 300 °C

Authorized licensed use limited to: Purdue University. Downloaded on September 08,2021 at 16:24:56 UTC from IEEE Xplore. Restrictions apply.

This article has been accepted for inclusion in a future issue of this journal. Content is final as presented, with the exception of pagination.

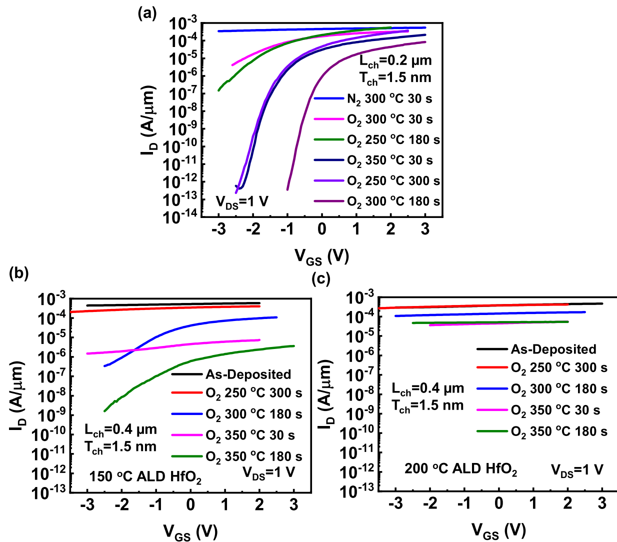

Fig. 7. (a) I_D–V_{GS} characteristics at V_{DS} of 1 V of top-gate In_2O_3 transistors with different annealing conditions. I_D–V_{GS} at V_{DS} of 1 V of top-gate In_2O_3 transistors with different annealing conditions with HfO_2 gate oxide deposited by ALD at 120 °C, (b) 150 °C, and (c) 200 °C.

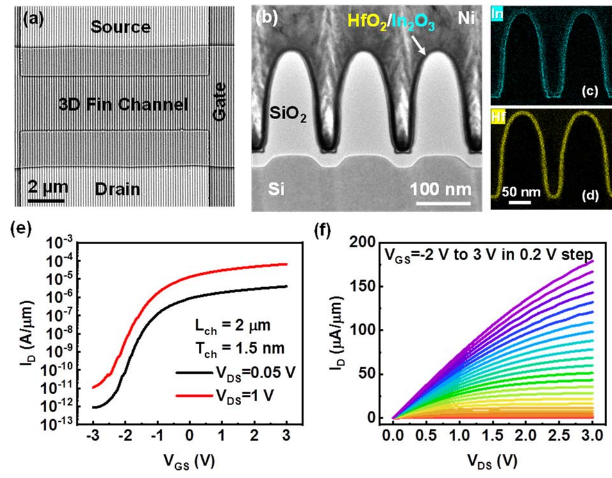

Fig. 8. (a) SEM image of an In_2O_3 3-D Fin transistor with top-gate structure. SiO_2 fin structures were fabricated by SEMATECH. (b) TEM image of a new type of 3-D Fin transistor with top-gate structure and In_2O_3 channel. EDX mapping under HAADF STEM of (c) In and (d) Hf, showing the conformal coating around the fin structure by ALD. (e) I_D–V_{GS} and (f) I_D–V_{DS} characteristics of an In_2O_3 3-D Fin transistor with L_{ch} of 2 μm and T_{ch} of 1.5 nm.

for 3 min. This device has a maximum I_D of 397 μA/μm and SS of 84.6 mV/decade. The small SS at the subthreshold region indicates a high-quality oxide/semiconductor interface. The interface trap density D_{it} at the sub-threshold region is estimated to be ~5-6 × 10^{12}/cm^2 eV. D_{it} at the HfO_2/In_2O_3 interface in a top-gate device is much larger than that in a back-gate device. The main difficulty for the integration of top-gate on the ALD In_2O_3 channel is from the ALD HfO_2 process. Hf-O bond with dissociation energy of 801 kJ/mol is much more stable compared to the In-O bond of 346 kJ/mol. ALD of HfO_2 on In_2O_3 generates more O vacancies in In_2O_3 and induces much more charge density. Meanwhile, it also degrades In_2O_3 film and HfO_2/In_2O_3 interface quality. Appropriate O_2 annealing can fill these O vacancies and heal most of the defects from the process so that SS of top-gate devices can be improved. To further improve the oxide/semiconductor interface quality, a top gate oxide or interfacial layer with low bond dissociate energy is preferred, and a lower interface trap density may be achieved. For example, Al-O has dissociation energy of 512 kJ/mol, and Mg-O has dissociation energy of 394 kJ/mol.

Fig. 7(a) shows the transfer characteristics at V_{DS} of 1 V of top-gate In_2O_3 transistors with different annealing conditions where the ALD HfO_2 was grown at 120 °C. As-fabricated devices, without annealing or devices annealed in the N_2 environment, cannot be turned off, the reason why these devices cannot be turned off is not just due to the high carrier density because the drain current density here is smaller than previous reported values in devices with similar dimensions [15]. Thus, the poor switching characteristics are also partly due to the high trap density at the HfO_2/In_2O_3 interface, which is generated during the ALD HfO_2 process. Devices annealed in O_2 show well-behaved switching on/off characteristics, suggesting that O_2 is necessary to heal these defects, also indicating that these defects are likely to be O deficiencies.

Therefore, from the above experimental observation, it is speculated that the deposition of HfO_2 by ALD generates defects at the HfO_2/In_2O_3 interface, most likely because the pulse of Hf precursor (TDMAHf) takes oxygen atoms away from In_2O_3, leading to the formation of oxygen vacancies at HfO_2/In_2O_3 interface. Such defects can only be healed in an O_2 environment by O_2 annealing. Such a process also depends on the annealing time, as shown in Fig. 7(a). It is also found that devices with O_2 annealing at 250 °C have higher I_D than devices with O_2 annealing at 300 °C with a similar threshold voltage (V_T). Therefore, low-temperature O_2 annealing is preferred to maintain high mobility.

Fig. 7 presents the I_D–V_{GS} characteristics at V_{DS} of 1 V of top-gate In_2O_3 transistors with O_2 annealing and with HfO_2 gate oxide deposited by ALD at (a) 120 °C, (b) 150 °C, and (c) 200 °C. As we can see, the on/off ratio of the devices degrades significantly with higher temperature HfO_2 ALD process and indicates that much more defects are generated at higher ALD temperature most likely due to the stronger reaction between TDMAHf and In_2O_3. All these detailed experiments offer a consistent picture of the challenge of integration of ALD HfO_2 on top of In_2O_3.

Fig. 8(a) shows the scanning electron microscopic (SEM) image of an In_2O_3 3-D Fin transistor with top-gate structure, capturing the gate metal, source/drain contacts, and the fin structures. Fig. 8(b)–(d) presents the transmission electron microscope (TEM) image and energy-dispersive X-ray spectroscopic (EDX) mapping under high-angle annular dark-field imaging (HAADF) scanning transmission electron microscope (STEM) of an In_2O_3 3-D fin transistor. ALD In_2O_3 channel with T_{ch} of 1.5 nm is conformally coated on top of SiO_2 fin structures with a fin height of 180 nm and a fin pitch of 130 nm, as shown in the EDX element mapping of Hf and In. Fig. 8(e) shows I_D–V_{GS} characteristics of an In_2O_3 3-D Fin transistor with L_{ch} of 2 μm and T_{ch} of 1.5 nm, exhibiting well-behaved transfer characteristics. Fig. 8(f) shows the

Authorized licensed use limited to: Purdue University. Downloaded on September 08,2021 at 16:24:56 UTC from IEEE Xplore. Restrictions apply.

This article has been accepted for inclusion in a future issue of this journal. Content is final as presented, with the exception of pagination.

corresponding I_D–V_{DS} characteristics with a maximum I_D of 180 μA/μm, normalized by device width, which is about two times larger than that from its top-gate planar counterpart. The 3-D fin structure provides an effective approach to increase the drive current without increasing the device area. The ultrathin channel thickness and the top-gate non-self-align structure with a large link resistance make I_D smaller than those from back-gate planar devices.

IV. Conclusion

In summary, high-performance 3-D Fin transistors and integrated circuits based on BEOL compatible oxide semiconductors by ALD are demonstrated. High mobility of 113 $cm^2/V \cdot s$ and high maximum drain current of 2.5 mA/μm are achieved. The demonstration of 3-D devices and integrated circuits suggests that ALD oxide semiconductors and devices have their unique advantages over sputtering films and are promising toward BEOL-compatible monolithic 3-D integration for 3-D integrated circuits.

References

[1] K. Nomura, A. Takagi, T. Kamiya, H. Ohta, M. Hirano, and H. Hosono, "Amorphous oxide semiconductors for high-performance flexible thin-film transistors," *Jpn. J. Appl. Phys.*, vol. 45, no. 5, pp. 4303–4308, Apr. 2006, doi: 10.1143/JJAP.45.4303.

[2] T. Kamiya and H. Hosono, "Material characteristics and applications of transparent amorphous oxide semiconductors," *NPG Asia Mater.*, vol. 2, no. 1, pp. 15–22, Jan. 2010, doi: 10.1038/asiamat.2010.5.

[3] S. Datta, S. Dutta, B. Grisafe, J. Smith, S. Srinivasa, and H. Ye, "Back-end-of-line compatible transistors for monolithic 3-D integration," *IEEE Micro*, vol. 39, no. 6, pp. 8–15, Nov. 2019, doi: 10.1109/MM.2019.2942978.

[4] S. Li *et al.*, "Nanometre-thin indium tin oxide for advanced high-performance electronics," *Nature Mater.*, vol. 18, no. 10, pp. 1091–1097, Oct. 2019, doi: 10.1038/s41563-019-0455-8.

[5] S. Samanta, K. Han, C. Sun, C. Wang, A. V.-Y. Thean, and X. Gong, "Amorphous IGZO TFTs featuring extremely-scaled channel thickness and 38 nm channel length: Achieving record high $Gm,_{max}$ of 125 μS/μm at V_{DS} of 1 V and I_{ON} of 350 μm," in *Proc. IEEE Symp. VLSI Technol.*, Jun. 2020, doi: 10.1109/VLSITechnology18217.2020.9265052.

[6] W. Chakraborty, B. Grisafe, H. Ye, I. Lightcap, K. Ni, and S. Datta, "BEOL compatible dual-gate ultra thin-body W-doped indium-oxide transistor with I_{on} = 370μA/μm, SS = 73 mV/dec and I_{on} /I_{off} ratio > 4×109," in *Proc. IEEE Symp. VLSI Technol.*, Jun. 2020, doi: 10.1109/VLSITechnology18217.2020.9265064.

[7] S. Li, C. Gu, X. Li, R. Huang, and Y. Wu, "10-nm channel length indium-tin-oxide transistors with I_{on} = 1860 μA/μm, G_m = 1050 μS/μm at V_{ds} = 1 V with BEOL compatibility," in *IEDM Tech. Dig.*, Dec. 2020, pp. 905–908, doi: 10.1109/IEDM13553.2020.9371966.

[8] J. Wu, F. Mo, T. Saraya, T. Hiramoto, and M. Kobayashi, "A monolithic 3D integration of RRAM array with oxide semiconductor FET for in-memory computing in quantized neural network AI applications," in *Proc. IEEE Symp. VLSI Technol.*, Jun. 2020, pp. 1–2, doi: 10.1109/VLSITechnology18217.2020.9265062.

[9] S. Dutta *et al.*, "Monolithic 3D integration of high endurance multi-bit ferroelectric FET for accelerating compute-in-memory," in *IEDM Tech. Dig.*, Dec. 2020, pp. 801–804, doi: 10.1109/IEDM13553.2020.9371974.

[10] H. Fujiwara, Y. Sato, N. Saito, T. Ueda, and K. Ikeda, "Surrounding gate vertical-channel FET with a gate length of 40 nm using BEOL-compatible high-thermal-tolerance In-Al-Zn oxide channel," *IEEE Trans. Electron Devices*, vol. 67, no. 12, pp. 5329–5335, Dec. 2020, doi: 10.1109/TED.2020.3021996.

[11] M. Si *et al.*, "Indium–tin-oxide transistors with one nanometer thick channel and ferroelectric gating," *ACS Nano*, vol. 14, no. 9, pp. 11542–11547, Sep. 2020, doi: 10.1021/acsnano.0c03978.

[12] K. Han *et al.*, "First demonstration of oxide semiconductor nanowire transistors: A novel digital etch technique, IGZO channel, nanowire width down to 20 nm, and I_{on} exceeding 1300 μA/μm," in *Proc. IEEE Symp. VLSI Technol.*, Jun. 2021, pp. 1–2.

[13] M. Si *et al.*, "BEOL compatible indium-tin-oxide transistors: Switching of ultrahigh-density 2-D electron gas over 0.8 × 1014/cm^2 at oxide/oxide interface by the change of ferroelectric polarization," *IEEE Trans. Electron Devices*, vol. 68, no. 7, pp. 3195–3199, Jul. 2021, doi: 10.1109/TED.2021.3061038.

[14] M. Si *et al.*, "Why In_2O_3 can make 0.7 nm atomic layer thin transistors," *Nano Lett.*, vol. 21, no. 1, pp. 500–506, Jan. 2021, doi: 10.1021/acs.nanolett.0c03967.

[15] M. Si, A. Charnas, Z. Lin, and P. D. Ye, "Enhancement-mode atomic-layer-deposited In_2O_3 transistors with maximum drain current of 2.2 A/mm at drain voltage of 0.7 V by low-temperature annealing and stability in hydrogen environment," *IEEE Trans. Electron Devices*, vol. 68, no. 3, pp. 1075–1080, Mar. 2021, doi: 10.1109/TED.2021.3053229.

[16] M. Si, Z. Lin, A. Charnas, and P. D. Ye, "Scaled atomic-layer-deposited indium oxide nanometer transistors with maximum drain current exceeding 2 A/mm at drain voltage of 0.7 V," *IEEE Electron Device Lett.*, vol. 42, no. 2, pp. 184–187, Feb. 2021, doi: 10.1109/LED.2020.3043430.

[17] A. Charnas, M. Si, Z. Lin, and P. D. Ye, "Enhancement-mode atomic-layer thin In_2O_3 transistors with maximum current exceeding 2 A/mm at drain voltage of 0.7 V enabled by oxygen plasma treatment," *Appl. Phys. Lett.*, vol. 118, no. 5, Feb. 2021, Art. no. 052107, doi: 10.1063/5.0039783.

[18] M. Si, Z. Lin, Z. Chen, and P. D. Ye, "First demonstration of atomic-layer-deposited BEOL-compatible In_2O_3 3D fin transistors and integrated circuits: High mobility of 113 $cm^2/V{\cdot}s$, maximum drain current of 2.5 mA/μM and maximum voltage gain of 38 V/V in In_2O_3 inverter," in *Proc. IEEE Symp. VLSI Technol.*, vol. 2021, p. T2-4.

[19] D. A. Mourey, D. A. Zhao, J. Sun, and T. N. Jackson, "Fast PEALD ZnO thin-film transistor circuits," *IEEE Trans. Electron Devices*, vol. 57, no. 2, pp. 530–534, Feb. 2010, doi: 10.1109/TED.2009.2037178.

[20] H. Y. Kim *et al.*, "Low-temperature growth of indium oxide thin film by plasma-enhanced atomic layer deposition using liquid dimethyl(N-ethoxy-2,2-dimethylpropanamido)indium for high-mobility thin film transistor application," *ACS Appl. Mater. Interface*, vol. 8, no. 40, pp. 26924–26931, Oct. 2016, doi: 10.1021/acsami.6b07332.

[21] Q. Ma *et al.*, "Atomic-layer-deposition of indium oxide nano-films for thin-film transistors," *Nanosc. Res. Lett.*, vol. 13, no. 1, pp. 1–8, Dec. 2018, doi: 10.1186/s11671-017-2414-0.

[22] J. Lee *et al.*, "High mobility ultra-thin crystalline indium oxide thin film transistor using atomic layer deposition," *Appl. Phys. Lett.*, vol. 113, no. 11, Sep. 2018, Art. no. 112102, doi: 10.1063/1.5041029.

[23] J. Sheng *et al.*, "Amorphous IGZO TFT with high mobility of ∼70 cm^2/(V s) via vertical dimension control using PEALD," *ACS Appl. Mater. Interface*, vol. 11, no. 43, pp. 40300–40309, Oct. 2019, doi: 10.1021/acsami.9b14310.

Authorized licensed use limited to: Purdue University. Downloaded on September 08,2021 at 16:24:56 UTC from IEEE Xplore. Restrictions apply.